Structures 63 (2024) 106428

Contents lists available at ScienceDirect

Structures

journal homepage: www.elsevier.com/locate/structures

An integrated digital design and construction approach for falsework-minimal masonry vaults

Robin Oval [a,*], Rafael Pastrana [a,b], Edvard P.G. Bruun [a], Vittorio Paris [c], Salvador Gomis Aviño [d], Sigrid Adriaenssens [a], Wesam Al Asali [e]

[a] Form Finding Lab, Department of Civil and Environmental Engineering, Princeton University, Princeton, USA
[b] School of Architecture, Princeton University, Princeton, USA
[c] Department of Engineering and Applied Sciences, University of Bergamo, Bergamo, Italy
[d] Bóveda Tabicada, Valencia, Spain
[e] School of Architecture and Design, IE University, Segovia, Spain

ARTICLE INFO

Keywords:
Structures
Shells
Construction
Centering
Guidework
Craft
Form finding
Augmented reality

ABSTRACT

Masonry vaults, mechanically efficient structures, are challenging to build because they require significant tailored falsework as temporary structures for centering, guidework, and scaffolding, which decreases construction productivity and increases financial cost and environmental impact. Traditional building techniques combined with recent digital technologies can eliminate such temporary construction. An integrated digital design and construction approach that leverages the benefits of four construction strategies (namely, thin-tile vaulting, loxodrome tessellation, augmented reality, and prefabricated spine) within a 4D funicular design framework is presented in this paper and illustrated by a large-scale demonstrator, *innixAR*. This structure demonstrates that the combination of the vernacular craft of thin-tile vaulting with augmented reality technology to produce a digital guidework, informing a 4D funicular design process that considers the entire construction sequence from a prefabricated spine, minimizes the required falsework, making the construction of masonry vaults more efficient and affordable. This approach is benchmarked against alternative conventional vault falsework. Combining thin-tile vaulting and prefabricated spine allowed a reduction of 82% of the falsework mass, making transport lighter. Whereas combining digital guidework and prefabricated spine allowed a reduction of 91% of the falsework elements, making assembly faster. This research contributes to the development of structures that are efficient both mechanically and constructionally.

1. Introduction

1.1. Context

The construction sector globally has shown 1% yearly productivity growth over the last 20 years, as opposed to 2.8% for the rest of the economy, and 3.6% in manufacturing specifically, resulting in a cost of $1.6 trillion per year [1]. Because the construction industry is one of the least digitized sectors in the world, several levers for action were identified, including: rethinking design and engineering processes; infusing digital technology, new materials, and advanced automation; improving on-site execution; and reskilling the workforce. The construction sector relies on massive unskilled intensive labor worldwide, which leads to economic and social abuse in the industry [2]. Leveraging digital technologies on the construction site to affordably build low-carbon structures with higher productivity can contribute to a positive impact on the economy, environment, and society. A main challenge lies in the productivity lost due to temporary construction works. For reinforced concrete structures, falsework, mainly timber formwork on scaffold as mold for casting concrete, accounts for 40% to 60% of the cost of the structure [3,4].

1.2. Problem statement

Masonry vaults are by design geometrically and mechanically efficient structures, as they withstand external loads through a compression-only structural behavior [5]. With common thickness-to-span ratios around and below 1:100, similar to an eggshell, these structures require low material quantities, without relying on tensile resistance [6]. However, building such structures is challenging due to the complexity of their doubly curved forms [7]. Erecting a masonry

* Corresponding author.
E-mail address: r.oval@tudelft.edu (R. Oval).

https://doi.org/10.1016/j.istruc.2024.106428
Received 9 February 2024; Received in revised form 26 March 2024; Accepted 14 April 2024
Available online 22 April 2024

Fig. 1. The innixAR prototype of a masonry vault demonstrating how to design and build for minimal falsework, leveraging 4D funicular design, thin-tile vaulting, loxodrome tessellation, augmented reality, and prefabricated spine.

vault usually requires the provision of different types of falsework, consisting mainly in the centering, a temporary structure that supports the vault during construction only, before the vault is completed and stable on its own. This centering, made of a combination of standard and custom wood or metal elements that fill the volume enclosed by the vault, requires careful design, planning, assembly, and disassembly, also called decentering [8,9]. Decentering, the lowering of the centering, is a critical, sudden, and dangerous step that aims at the vault being self-supporting at once. Such temporary construction works make vaults unaffordable to build, both from a material consumption and a construction efficiency and safety perspective.

Traditional techniques for masonry construction offer solutions to mitigate the use of centering for masonry vaults. Such strategies include: corbelling [10–12], pitched vaulting [13–17], thin-tile vaulting [18–20], rib networks [7,21–23], loxodrome tessellations [24–26], interlocking voussoirs [27–29], or cable systems [7,30]. More details about these strategies can be found in [31].

Digital fabrication technologies have shown the potential of building masonry structures without centering. Promising examples encompass the construction of walls with a mobile robotic arm [32]; drone construction of small-scale voxelated masonry structures, walls, and vaults, made of interlocking blocks [33]; cooperative robotic construction of pavilion-scale masonry vaults [34–37]; augmented construction of vertical masonry structures [38]; collaborative augmented robotic construction of vertical structures, with augmented manual gluing and robotic brick positioning [39–41]; augmented reality to visualize the positioning of the falsework and the construction of the vault through a tablet [42]; and augmented reality for the construction of a thin-tile vault staircase through a head-mounted device [43].

1.3. Research objective

This research aims to minimize falsework (i.e., scaffold, centering, guidework) in the construction of masonry vaults, enabled by the combination of historical construction strategies and novel design and construction digital technologies to achieve economic and efficient construction.

This research is presented and exemplified through the demonstrator *innixAR*, shown in Fig. 1, a masonry vault with timber ribs, an application of an integrated approach to improve construction efficiency and economy through the combination of vernacular craft with modern digital design and construction technologies. This pavilion-scale structure is located in the garden of the campus of IE University in Segovia, on a 5 m × 5 m × 3 m triangular footprint shown in Fig. 2. The architectural goals of this structure are to provide a shaded space for staff and students to gather while framing three scenes from the natural and historical surroundings of the site: the sinuous path of the Eresma River, an ancient monastery in Segovia, and the hills over the central Spanish plateau.

1.4. Contributions and paper outline

In this paper, the integrated digital design and construction approach to minimize falsework is explained, tested, and quantified. In Section 2, the strategies combined for falsework minimization are presented, namely, thin-tile vaulting, loxodrome tessellation, augmented reality, and prefabricated spine. In Section 3, the design process for centering-free construction of masonry vaults, so-called 4D funicular design, tackling the form, tessellation, thickness, and assembly sequence, is detailed. 4D funicular design extends state-of-the-art 3D funicular form finding, which focuses on the equilibrium of the final shape of the structure. In Section 4, the construction process of the demonstrator is described, including the prefabrication of the spine and the use of augmented reality for construction. In Section 5, the falsework economy is assessed, with falsework mass, embodied carbon, construction time, and financial cost as metrics. This approach is compared to alternative construction scenarios to evaluate the respective contribution of each strategy used.

2. Falsework minimization approach

To minimize falsework for masonry vault construction, several strategies are leveraged to build faster with reduced centering and guidework:

- **thin-tile vaulting**: using the material properties of lightweight tiles and fast-setting mortar to reduce vault centering (Section 2.1);
- **loxodrome tessellation**: using a masonry tessellation with transverse interlocking tiles to reduce delay due to mortar setting (Section 2.2);
- **digital guidework**: using augmented reality to visualize digital guidework instead of building a physical one (Section 2.3);
- **prefabricated spine**: using a rationalized network of stay-in-place internal ribs instead of a complex boundary centering (Section 2.4).

These construction strategies inform the process of *4D funicular design* to find the vault form, masonry tessellation, assembly sequence, and cross-section thickness that can be built with minimal falsework. 4D funicular design extends 3D funicular form finding, by comprehensively including form, tessellation, thickness, and assembly sequence, to achieve a structure in spatial equilibrium throughout construction time.

2.1. Thin-tile vaulting

Thin-tile vaulting is a technique based on the assembly of lightweight thin tiles with a fast-setting mortar into composite layers, often built arch by arch, to form a vault, an arch, a staircase, a floor, a roof, or a tunnel. In this paper, the craft of thin-tile vaulting is used, as practiced today in 21st-century Spain. This technique eliminates the bulk of the centering thanks to the sufficient early bond capacity of the mortar with the tiles. This technique was popular in Medieval Spain, and later brought to the US by Rafael Guastavino in the 19th century [44]. It remains popular today with numerous examples in Cuba, Syria, Rwanda, Jordan, and Spain [20], as well as among academics, as documented by [19].

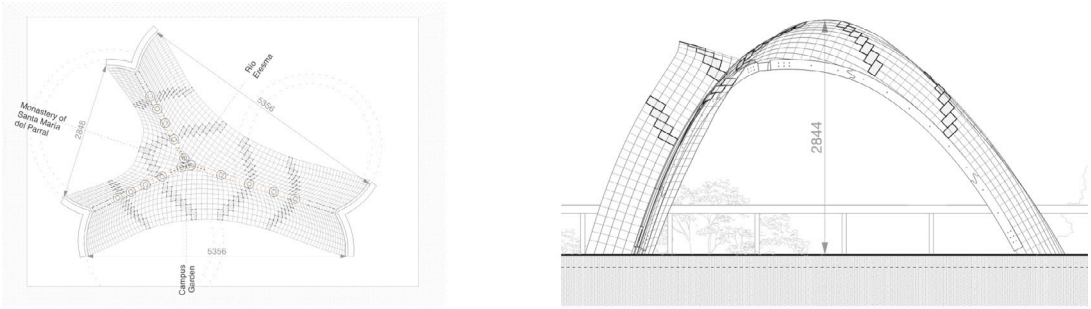

(a) Plan (b) Elevation

Fig. 2. The innixAR demonstrator within architectural site context (main dimensions shown in mm).

2.2. Loxodrome tessellation

A loxodrome tessellation features bricks that run transversely to a regular staggered pattern [26]. Such bricks are clamped by the previous masonry arch, cantilevering, and offering support to the next masonry arch. During the construction of a masonry vault, the setting time of the mortar must be respected when adding successive arches, which requires pausing or delaying by alternating work on different parts of the vault. In this paper, a loxodrome tessellation is used, reducing the need to rely on the mortar setting time and to wait for it to build up strength during construction. These intermediary supports allow building an arch into sub-arches without a full arch centering. These tessellations were used for Persian domes, in Iran with the Ardestan Mosque (1088) and the Isfahan Mosque (1158), or in Turkey with the Great Mosque in Eski Malatya (1224) [45]. The interaction between the Timurid Empire (ca. 15th century) and the Italian Renaissance (ca. 15th-16th centuries) [24] led to the Santa Maria del Fiore Cathedral in Florence, built by Brunelleschi and Sangallo (1436) without centering [25,26]. Loxodrome tessellations are still used today in the construction of vaults in Mexico [46], as a hybrid technique between thin-tile vaulting and pitched vaulting [47–49].

2.3. Digital guidework

Traditionally thin-tile vaulting guidework is necessary to allow the masons to control and correct the shape of the vault during assembly, made from rigid boards, beams, or flexible rods, in timber, metal, or composites [8,9,50]. In this paper, a digital guidework is employed using augmented reality to visualize the vault's shape and tessellation through a head-mounted device for the mason with a set of markers installed on-site. The guidework is digitized, saving the time and labor to design, produce, install, and position it [42,43].

2.4. Prefabricated spine

The centering of masonry vaults, including thin-tile vaults, usually relies on an initial set of arches, along the boundaries, the ribs, and the creases of the vault. For a vault with doubly-curved unsupported boundary arches, a boundary centering would have to follow the complex curvature of the arch itself, be supported laterally with shoring against the asymmetrical thrust of the rest of the vault during construction, and be more expensive to build. In this paper, a central spine is adopted for this initial centering. This spine follows the medial axis of the vault and acts as a stay-in-place central rib, consisting of a system of connected planar arches, which are prefabricated for accurate and simple assembly. The development of ribbed domes and vaults progressed first through Islamic-Moorish architecture of the Omeyyades (ca. 7th-11th century) [21–23], and then Romanesque-Gothic architecture (ca. 11th-16th century) [7,51]. Ribs have been introduced in vaults to provide a hierarchy in these structures. They allow a significant reduction of the centering, as the ribs are assembled first, on centering that is lighter as it does not need to support the full vault, before assembling the rest of the vault as brick courses on simpler centering spanning between the ribs [7]. Particularly, vaults like the Al-Ukhaidir Fortress built in Iraq (775) rely on such arches that are prefabricated out of plaster [52]. The LightVault prototype (2020) also relied on an initial central arch as a spine, built without centering thanks to collaborative robotic assembly [34]. As a result, this centering is shorter, lighter, and simpler than a shored doubly-curved boundary centering. This influences the construction process, building from the inside out as opposed to the outside in. It also steers the 4D funicular design and its sequential form-finding process that takes into account the phases of construction.

Fig. 3 highlights the complementary contributions of these different strategies. With thin-tile vaulting, the surface centering can be reduced to a boundary centering and a physical guidework, while the loxodrome tessellation strengthens the connection between successive masonry arches, particularly during construction. With augmented reality, the physical guidework can be eliminated by turning it into a digital one. The remaining arch centering can be simplified, from doubly-curved boundary centering to shorter planar centering in the form of ribs acting as a stay-in-place prefabricated medial spine, simplifying the design, fabrication, and assembly of the centering, and using it as a permanent component. The combined benefits of these construction strategies (i.e., thin-tile vaulting, loxodrome tessellation, digital guidework, and prefabricated spine) inform the 4D funicular design process, from which stem the form, tessellation, thickness, and assembly sequence of the vault.

3. 4D funicular design

The initial architectural intent of framing the three surrounding architectural and natural scenes of the site led to the design of a vault based on three arches. To minimize the vault's falsework, the design process of the form, tessellation, thickness, and assembly sequence of the structure is informed by the craft and technology of the strategies discussed in Section 2. To achieve a masonry vault that is in equilibrium, in compression, without centering throughout the construction process, *4D funicular design* is introduced here, with the vault analyzed, designed, and built as a succession of arches. 4D refers to the fourth dimension of time, as an addition to the three dimensions that describe space.

Throughout the digital modeling process, the vault is represented as a mesh of quadrilateral faces. Such a quad mesh is organized as strips (series of faces) and polyedges (series of edges). This data structure captures the organization of the masonry tessellation with its continuous tile and brick courses. The proposed 4D funicular design process consists of three steps: topological design (Section 3.1); sequential form finding (Section 3.2); and vault tessellation (Section 3.3).

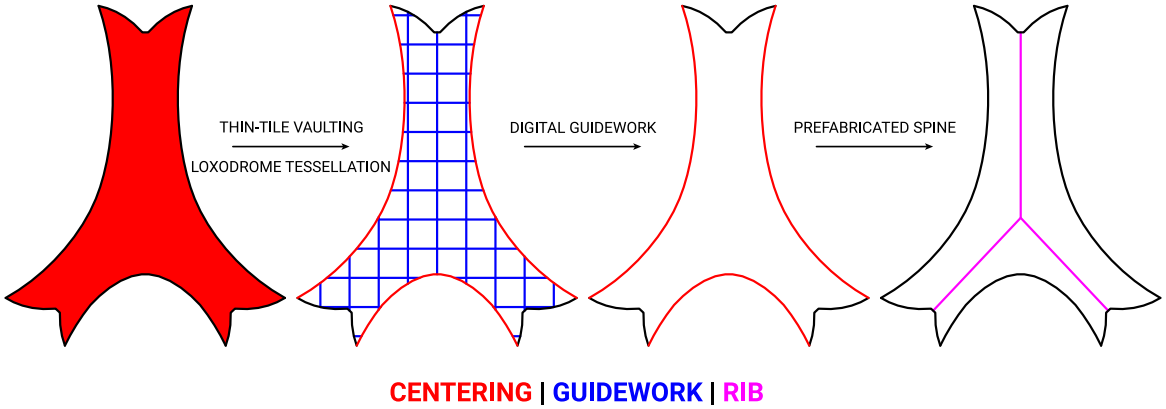

Fig. 3. Combined strategies for minimizing falsework from a full vault centering to a digital guidework and a stay-in-place prefabricated central rib called spine.

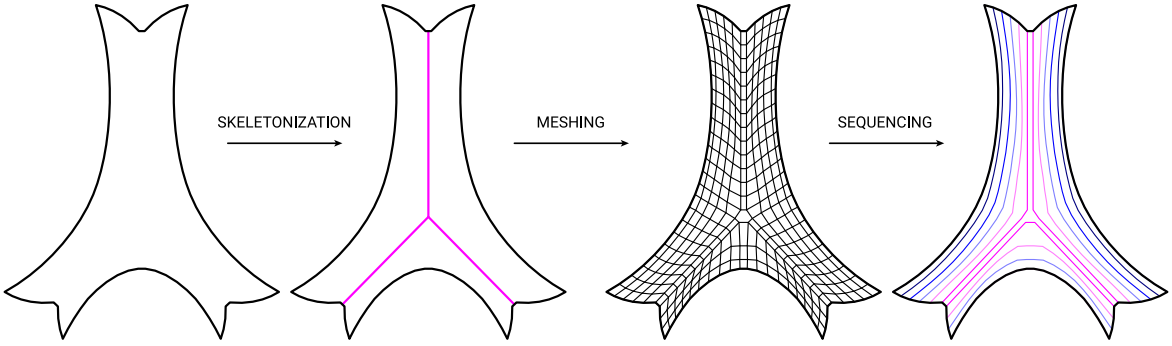

Fig. 4. Generation of the topology of the pattern and assembly sequence based on a spine as a modified topological skeleton.

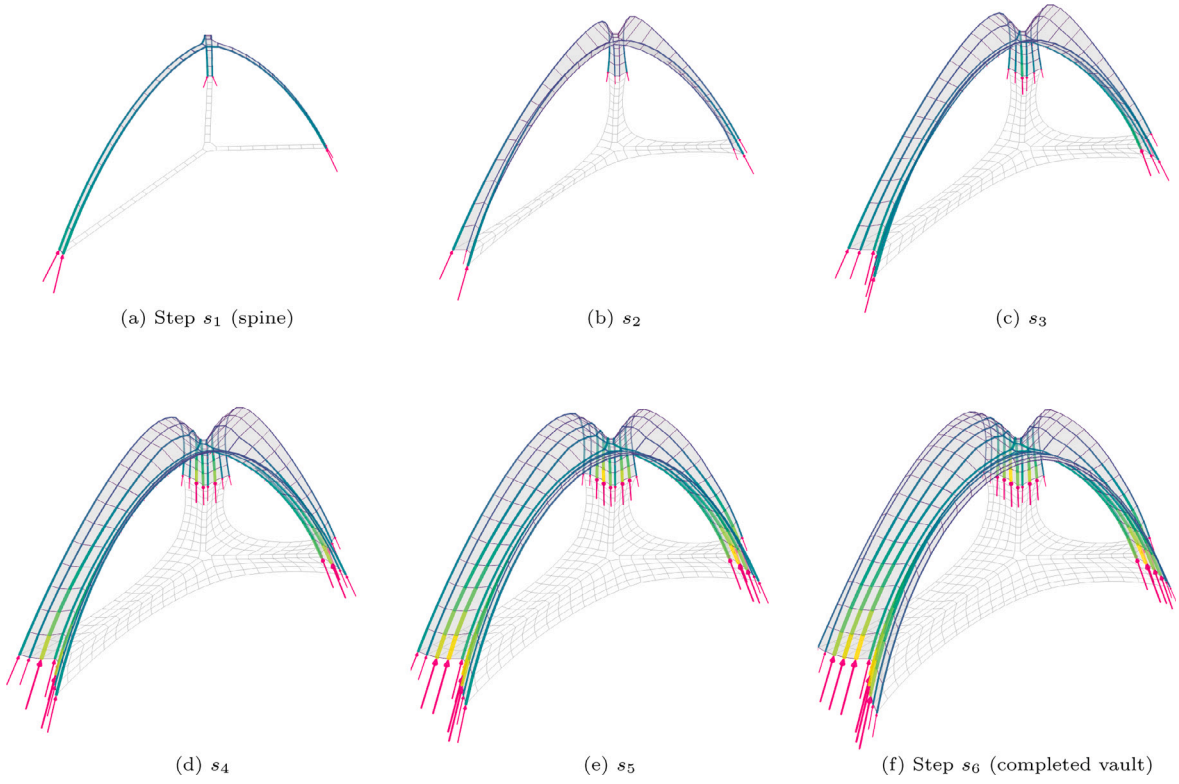

Fig. 5. Sequential form-finding of the spine and the masonry vault, modeled as a sequence of thrust networks calculated over six consecutive constrained optimization steps, s_1 to s_6.

3.1. Topological design

The different steps of the topological generation process are shown in Fig. 4. The process involves the generation of a coarse quad mesh from the medial axis of the surface, and its densification for the computation of the assembly sequence [53].

3.1.1. Pattern topology

The topology of the structure is designed based on the boundary and support conditions of the vault. A fully supported vault can be constructed arch per arch, or ring per ring, starting from the supports, and potentially a set of additional arches built from a centering. To minimize the total length of this arch network, the medial axis, also called topological skeleton, which corresponds to the set of points that are equidistant to the surface boundaries [54], serves as the base to form a spine for the vault, building inside-out (*skeletonization* in Fig. 4). The medial axis is simplified to straight branches that connect the supports to be interpreted as a network of planar arches. The rationalized arches are then planar elements, as opposed to complex doubly-curved boundary ones [55], with approximately half the length. This spine approach also provides clear paths for easier unobstructed access to the construction site, with access scaffolding, as for the innixAR demonstrator, mechanized platforms, or automated machines. It also removes the challenge of closing the vault by accurately fitting a final keystone. Using the subdivision obtained by the spine, a coarse mesh is obtained and densified (*meshing* in Fig. 4). For the innixAR demonstrator, the spine consists of three arches stemming from the three supports and meeting at the center of the vault.

3.1.2. Assembly sequence

A post-design approach for computing assembly sequences of vaults involves trying different paths in a decision tree. Searching for self-stable parts of the vault to build first naturally yields complete arches or rings [55,56]. This construction logic of building the vault arch by arch is embedded in 4D funicular design. The spine consists of initial arches that serve as support for the next ones. The polyedges that are topologically parallel to the spine are considered as a series of virtual arches that represent the main curves of the masonry course, sorted based on their distance to the spine (*sequencing* in Fig. 4). For the innixAR demonstrator, the key steps s of the assembly sequence are s_1 for starting from the spine, and s_4 and s_6 to complete the short and long spans of the vault, respectively.

Then, a construction-aware shape for the vault can be sequentially form found by including information about the assembly steps.

3.2. Sequential form finding

The primary objective of 4D funicular form finding is to generate a design that stands in compression under self-weight during and after construction. The equilibrium of the vault is modeled as a thrust network using limit analysis [5,57]. This design is the result of a chain of constrained form-finding problems solved with an auto-differentiable Force Density Method (DFDM) [58–60]. For the innixAR demonstrator, the sequential form finding is applied over six construction steps s, shown in Fig. 5, from the spine at s_1 to the completed vault at s_6.

3.2.1. Prefabricated spine

The spine, form found during step s_1 in Fig. 5(a), has a maximum height set to 2.3 m to allow the builders to reach from a standard scaffolding platform, and has a fixed horizontal projection to fabricate it from planar boards. For all the subsequent steps, the geometry of the spine is fixed by adding virtual supports to the model. This induced discrepancy with the actual support conditions helps find a sequence of thrust networks with little deviation from each other. The residual forces in the virtual supports must be carried by the spine thanks to its bending capacity.

3.2.2. Masonry arches

The masonry vault is form found by adding a sequence of thrust networks on each side of the vault until completion, from steps s_2 to s_6 in Fig. 5. The extension of the thrust network is posed as a constrained form-finding problem. The objective of each constrained form-finding problem is to compute the thrust network at the given assembly step that satisfies a set of structural and constructive design goals. Therefore, an optimization problem is formulated, where each goal g_k is weighted by a factor w_k and aggregated in a loss function $\mathcal{L}$:

$$\begin{aligned} \min \quad & \mathcal{L}(\mathbf{q}, \mathbf{z}_s) = \sum_k w_k \, g_k \\ \text{s.t.} \quad & \mathbf{q} < \mathbf{0} \\ & \mathbf{z}_s \geq \mathbf{0} \end{aligned} \tag{1}$$

where the design parameters are the force densities $\mathbf{q}$ of all the edges in the thrust network, and the vertical coordinates $\mathbf{z}_s$ of the nodes of the spine. To solve this optimization problem, the function $\mathcal{L}$ is minimized with the gradient-based optimizer L-BFGS [61]. The required gradients are obtained with automatic differentiation [62]. The force density parameters are bound to the negative domain to ensure a compression-only solution ($\mathbf{q} < \mathbf{0}$). At each assembly step s_i, the main goals, and their weights w_k marking their importance, are split between the ones applied to the new and the ones applied to the existing elements of the thrust network. The following goals are applied to the edges added at the current assembly step s_i:

1. *Enhanced arch stability* ($w_1 = 10$). The stability of the tiles of an arch being built is assured by the angle of the bond to the existing part of the vault until the arch is completed. The stability of the bond is increased by controlling the inclination of the interface, by prescribing a target angle α between the slope and the vertical. This goal is assigned to the edges on the transversal polyedges stemming from the node of the spine, as shown in Fig. 6. The values of α are linearly interpolated from 45° and 60° at the spine, for the long and short spans, respectively, to 75° at the boundary. The maximum value is based on vernacular vault construction with these specific mortar and tiles. The minimum values and the linear interpolation are design choices based on the aesthetics (vault profile) and function (covered area) of the resulting form.
2. *Uniform tile width* ($w_2 = 1$). To simplify later tessellation materialization, each assembly step should correspond to the addition of a similar number of arches with a unique tile width, aligning the force flow with the interfaces. Therefore, the normalized variance of the length of the transversal edges is minimized.

The following goals are applied to the nodes that already exist in the previous assembly step s_{i-1}:

3. *Small spine deformations* ($w_3 = 15$). As detailed in Section 3.2.1, the nodes representing the spine are considered fixed in assembly steps s_2 to s_6 to find consecutive thrust networks that are close to each other. The residual forces at these nodes result in non-funicular loading on the timber spine. The spine can withstand such loading thanks to its bending stiffness. However, the exerted thrust is lowered to reduce the stress level and deflections of the spine. To this end, the shape of the spine is updated at every assembly step to minimize the magnitude of the forces acting on it.
4. *Best-fit construction history* ($w_4 = 5$). From one assembly step to the next, the form-found thrust network can vary significantly in shape, especially after adding new elements. The masonry vault eventually has to contain the entire sequence of form-found thrust networks within its thickness to guarantee stability during construction. The greater the difference between consecutive thrust networks is, the thicker the vault must be. Therefore, the Euclidean distance between the position of each node at a given assembly step and its position in the previous one is minimized.

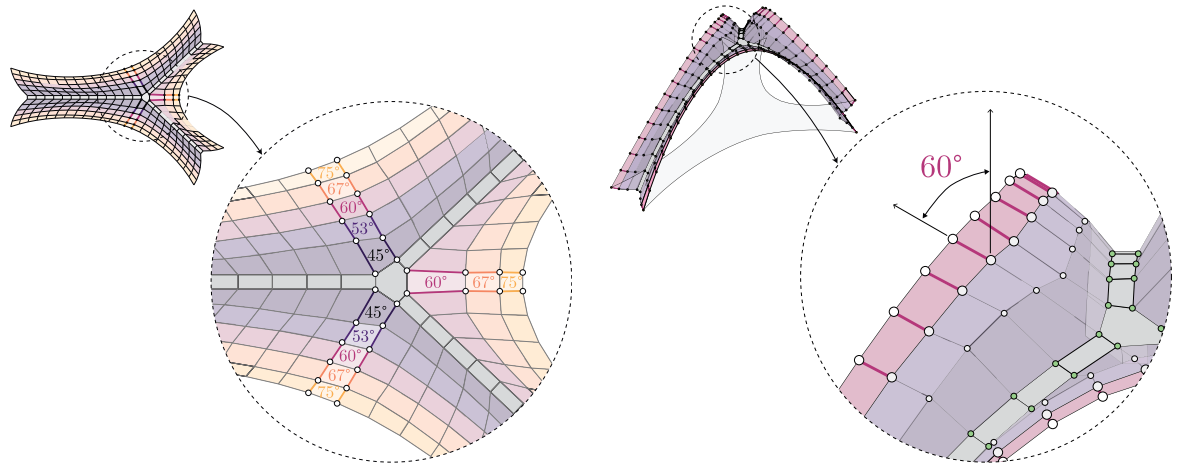

Fig. 6. Increasing arch stability through a set of target angles for surface slope goal in the successive thrust networks.

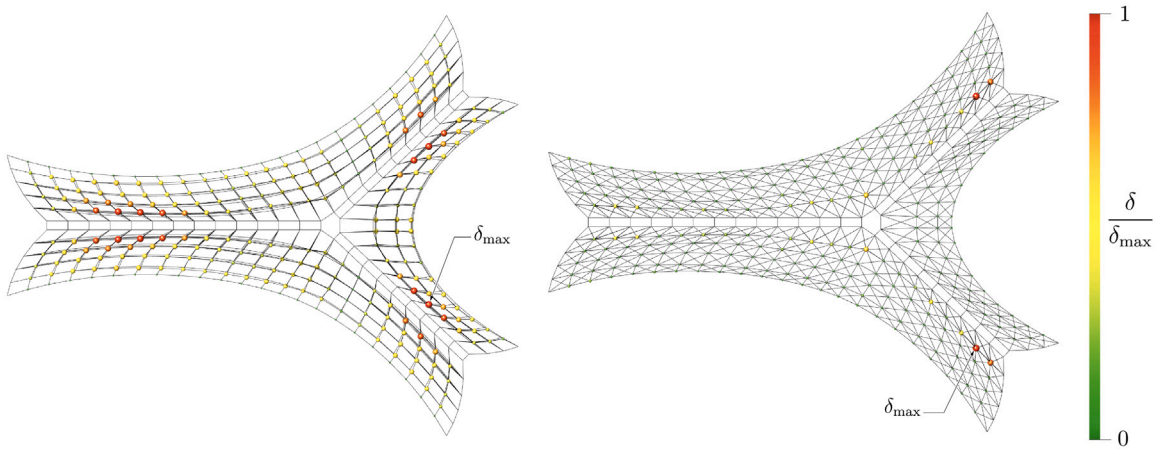

(a) Sequential form finding (δ_{avg} = 30 mm, δ_{max} = 70 mm) (b) Form fitting (δ_{avg} = 1 mm, δ_{max} = 5 mm)

Fig. 7. Distance δ between nodes and medial surface when superimposing the thrust networks generated with sequential form finding, before and after form fitting. This distance gives an upper bound for the half thickness of the first layer of the vault to be built without centering.

The sequence of form-found thrust networks generated with optimization then informs the selection of a structurally appropriate vault thickness.

3.2.3. Vault thickness

The final form-found thrust network at assembly step s_6 provides the medial surface of the first layer of the masonry vault. This final network is a best fit of the sequence of thrust networks generated at each assembly step, as a result of the sequential form-finding process. Each preceding thrust network must be contained between the intrados and the extrados of the vault to ensure mechanical stability during and after construction according to the lower-bound theorem of limit analysis for masonry vaults [5]. The superimposition of the thrust networks thus guides the selection of the vault thickness, which must be at least twice the maximum distance δ^j to the medial surface per node j and for all the generated thrust networks, to account for deviations on both sides of the medial surface during construction. As shown in Fig. 7(a), the average distance per node across steps s_2 to s_6 is δ_{avg} = 30 mm, with a maximum δ_{max} = 70 mm close to the spine.

With a target shape obtained from sequential form-finding, form-fitting is performed to find a lower thickness value for the vault to be stable under self-weight during construction [63–65]. Each thrust network s_2 to s_6 is triangulated to increase quantitatively and qualitatively the number of load paths to fit the target shape. Fig. 7(b) shows the new set of form-fitted thrust networks per assembly step and the distances between the nodes and the medial surface. The new average distance to the final shape is δ_{avg} = 1 mm, with a maximum δ_{max} = 5 mm. This new maximum thickness is lower than half of the thickness of the tiles (Section 4.2) and therefore the first layer of the vault can be built without centering. Furthermore, form-fitting demonstrates that sequential form finding as per Section 3.2.2 produces a conservative estimate of the required vault thickness that can be significantly reduced with further optimization.

3.3. Vault tessellation

The materialization of the masonry tessellation on the form-found surface must follow a set of requirements. Cutting tiles to create chamfers is time-consuming and interrupts the structural continuity of arches. Consequently, complete tiles courses are favored to minimize the number of tiles to cut. As a result of the constrained form finding, the thrust network offers a regular but not constant set of arches. The tile courses are thus produced following a constant curve offset from the spine on the surface based on ortho-geodesic curves [66]. However, the central node of the spine would induce kinks in the tile coursing and the resulting tessellation. Therefore, squinches, which are triangles in the vault, are used to smooth the kink. The dimensions of the squinches are tuned so that the tessellation fits the boundaries of the form-found

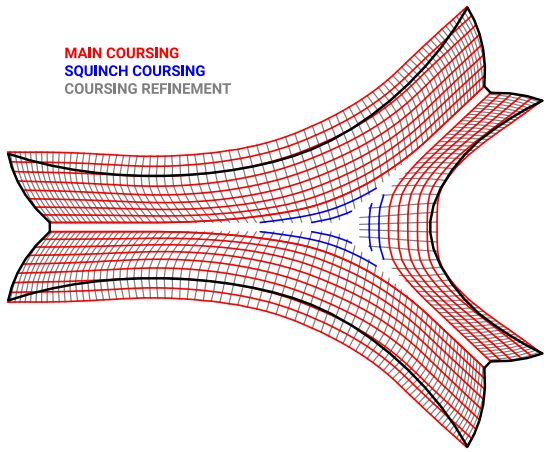

Fig. 8. Masonry coursing generation.

Table 1
Main geometrical dimensions of the vault after 4D funicular design.

Dimension	Value
Bounding box [m^3]	5.8 × 4.8 × 2.8
Unsupported boundary length (projected) [m]	23.3 (15.2)
Spine length (projected) [m]	10.2 (7.2)
Vault surface [m^2]	16.7 (9.2)
Vault enclosed volume [m^3]	16.4

surface with squinches as small as possible to minimize the number of tiles to cut. The resulting masonry coursing, shown in Fig. 8, has eight complete arch courses for each long span, two of them only partially covering the form-found shape, and five for the short span. Each squinch spans over three interrupted arch courses.

The curves with a constant offset are subdivided to obtain a quad mesh. The masonry tessellation is then computed by merging pairs of faces. First, transversal tiles are generated to produce the loxodromes, spaced by five tiles to break down the arches into sub-arches with a span of about 1 m. Double loxodromes, resulting in a cross pattern with variable spans for the sub-arches, are discarded to prevent unnecessary cutting without additional benefits. The loxodromes are oriented upward so that a loxodrome tile rests upon the previous one during the assembly process. Then, the rest of the tiles of the masonry tessellation are combined in the longitudinal direction in a checkerboard fashion to obtain a staggered pattern. Finally, the tessellation is thickened off the surface to obtain closed volumetric meshes representing the 3D tiles, as shown in Fig. 9 at three different assembly stages with the loxodrome tiles highlighted. As the mesh faces are not necessarily planar, the discrepancies between the adjacent flat tiles are solved by the mortar joint.

As a result of this 4D funicular design process, informed by the construction process aiming for minimal falsework, the main geometrical dimensions of the vault are reported in Table 1, used for financial and environmental assessment in Section 5.

4. Vault construction process

The innixAR demonstrator vault was constructed over six days, including preparation with the casting of the foundation and installation of the spine (Fig. 10(a)), augmented construction of the first layer (Figs. 10(b) and 10(c)), and addition of the second layer on the already-laid first layer (Fig. 10(d)). Preparation included the prefabrication and erection of the spine on-site, along with the construction of the masonry footing, anchored with steel reinforcement bars to the foundation, which consists of a 150 mm flat reinforced concrete slab on 50 mm of gravel with durability reinforcement.

Table 2
Theoretical material quantities of the masonry vault.

		Volume [m^3]	Density [kg/m^3]	Mass [kg]
First layer	Hollow thin tiles	0.407	1070	436
	Gypsum plaster	0.061	2300	140
Second layer	Solid thick bricks	0.651	1800	1173
	Cement mortar	0.081	2000	163
	Total	**1.14**	–	**1912**
	Per vault surface [$/m^2$]	0.0683	–	114
	Per covered area [$/m^2$]	0.124	–	208

4.1. Digital data

During the planning of the construction, several digital models containing different specific data were generated for the funicular shape (Fig. 11(a)), the masonry tessellation (Fig. 11(b)), the prefabricated spine (Fig. 11(c)), and the digital guidework (Fig. 11(d)). This seamless production and use of digital information, from design to construction, was possible because of augmented reality, utilizing a digital 3D model of the structure, as opposed to physical 2D plans.

4.2. Materials and layers

As any masonry and concrete construction technique, thin-tile vaulting requires above-freezing temperature, while humidity conditions are adapted through the water content of the plaster. The masonry units are made from fired clay, where the first layer of the vault consists of hollow thin tiles (225 mm × 100 mm × 25 mm) with a fast-setting gypsum plaster (10 mm per interface before pressing), acting as centering-formwork for the second layer of solid thick tiles (225 mm × 100 mm × 40 mm) placed on a bed of regular mortar with an approximate thickness of 5 mm, for a total masonry vault thickness of 70 mm. Fig. 12 features the cross-section of the vault with its combination of materials, and Table 2 provides the theoretical material weight of the vault, averaging 208 kg/m^2 (covered area).

4.3. Spine construction

The spine is a stay-in-place centering acting as a central rib. The spine is prefabricated off-site before on-site installation. Its deflection is checked during vaulting as the spine carries the required markers needed for augmented construction.

4.3.1. Fabrication

The spine is a tripod made of three planar timber arches, called legs, connected by a steel node, and to the foundation by a welded steel plate, shown in the exploded view in Fig. 11(c). All these elements are prefabricated and each leg pre-assembled. The steel node consists of three plates that are bent to connect the legs of the spine. The cross-section of the spine is a constant 90 mm wide and 120 mm deep rectangle. Each leg is made of 5 layers of 18 mm thick birch plywood boards. The layers are cut using a CNC machine. The depth of 120 mm is tuned to provide enough bending stiffness to reduce displacements during assembly, which was verified using finite element analysis of the loaded spine. The central layer of the spine features an upper extension of 30 mm to support and guide the positioning of the first course of tiles that form the crease of the vault. To facilitate transportation, the cut plywood layers are split into elements with a length of 50 to 200 cm, with smooth jigsaw joints, in a staggered organization from one layer to another to prevent the formation of continuous lines of structural weakness. The layers are glued and bolted together.

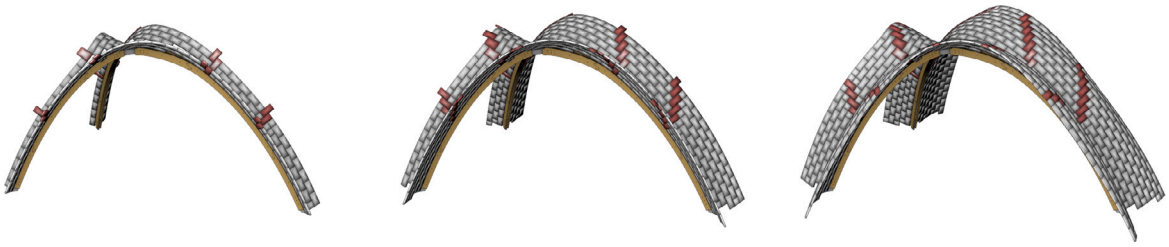

Fig. 9. Materialized masonry vault on the timber spine at three assembly stages with staggered tessellation and loxodrome tiles.

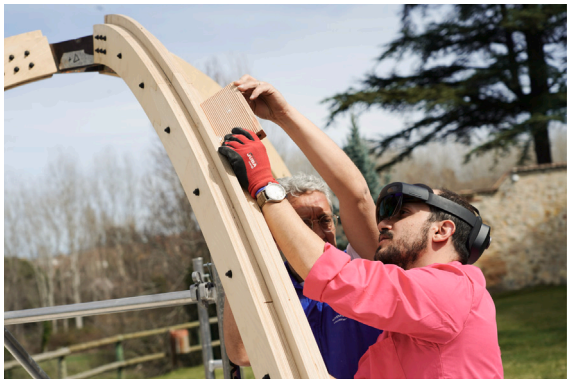

(a) Augmented planning (photo credit: Camila Zoe Gomez)

(b) Digital guidework

(c) Tile vaulting (photo credit: Roberto Arribas)

(d) Parallel construction (photo credit: Camila Zoe Gomez)

Fig. 10. The different construction stages of the vault.

4.3.2. Installation

Once the three legs are assembled off-site, they are bolted on-site to the steel node to form the spine, shown in Fig. 13. To guide the positioning of the spine, a triangle was marked on the concrete slab to position the three base points, which corresponded to the middle point of the intrados edge of the anchor steel plates. This process took about one hour on-site for three workers, using a scaffold platform with a pulley to carry the central node while connecting the legs. Once assembled, the spine is bolted to fin steel plates that are welded to anchor steel plates cast in the concrete foundation slab. Precise fabrication and positioning of the spine are crucial for aligning the physical and digital worlds for augmented construction.

4.3.3. Deflection

Form finding favors a compression-dominant behavior of the spine, minimizing its deflection without additional supports, as a stay-in-place centering and carrier of the markers for the digital-physical world registration. The vertical displacements of the spine are monitored during construction with a set of 18 equidistant reference points engraved on the underside of the spine, six per leg as shown in Fig. 14(a), by performing daily measurements with a laser of their vertical positions relative to the foundation slab. The measurements are taken every morning before the start of the construction activities of the day. This monitoring method does not capture lateral displacements, but these are reduced by alternating construction between the three sides of the vault to reduce asymmetrical loading and horizontal thrust. The measurements, plotted in Fig. 14(b), reveal a maximum average displacement under 10 mm, which is less than $1/200^{\text{th}}$ of their total span. At least 50% of the total displacement in the long leg (Leg 1) and 70% in the short ones (Legs 2 and 3) occurs right after the installation of the spine, due to the activation and sliding of the connections under initial loading. Afterward, the spine experiences additional displacements, when adding masonry, of 1 mm on average per day, which corresponds to the tolerance of the laser. These small displacements suggest that the masonry increases self-weight but also stiffens the structure, indicating that the vault works as a self-bearing element during construction.

4.4. Augmented vaulting

The use of augmented reality is primarily driven by two factors. Firstly, augmented reality offers a *digital guidework*, eliminating the need for physical guidework, usually a tedious but essential task to

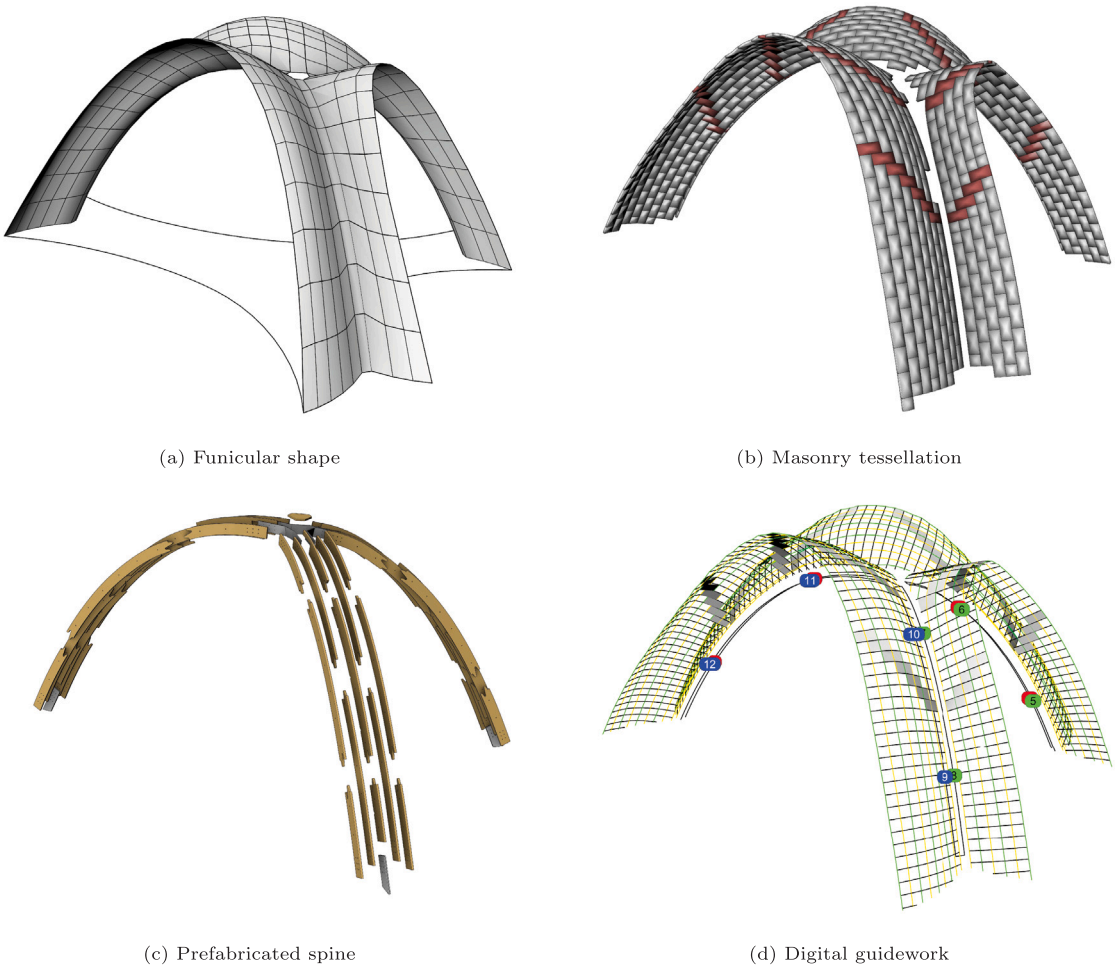

(a) Funicular shape (b) Masonry tessellation

(c) Prefabricated spine (d) Digital guidework

Fig. 11. The different digital models of the vault, from design to construction.

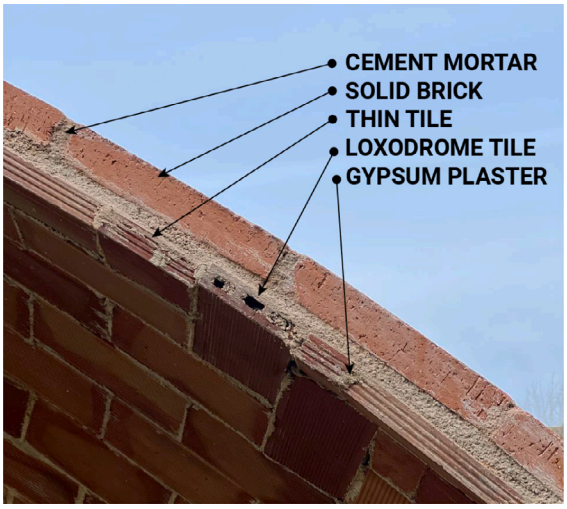

Fig. 12. Two-layer composite vault cross-section.

Fig. 13. Central connection detail with steel node, timber spine legs, and masonry squinches.

build such a geometrically complex vault precisely. Secondly, augmented reality empowers the builders, assisting while letting them adapt and make decisions on-site. Augmented craft permits dealing with diverse and variable materials like masonry and mortar, where unexpected challenges regularly occur on the construction site. Efficient construction relied both on the builder's experience and skills and embracing the augmented-reality technology.

4.4.1. Physical implementation

Augmented reality dispenses the need for physical guidework by providing a digital one. Physical guidework is usually made of a reusable lightweight scaffold supporting bent elements made of metal, wood, or plastic, which provide an outline of the vault in a few locations only, usually the main arches of the vault like the boundaries,

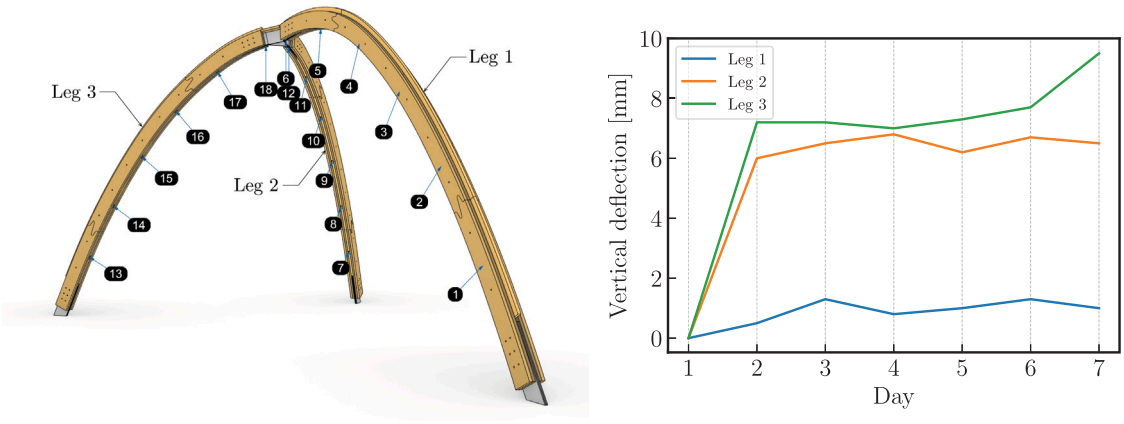

(a) Reference point location (b) Vertical deflections during construction

Fig. 14. Monitoring of the average vertical deflection of the legs of the spine during construction based on 18 reference points.

or as an orthogonal grid. The augmented reality model provides both a digital guide of the surface of the vault and its tessellation, the main masonry courses, and the transverse loxodrome tiles. Augmented reality is not used for the second layer, which consists of a regular staggered tessellation only, as it directly follows the first layer with an in-plane offset of half the width of a brick. Additionally, augmented reality is used to outline the position of the brick foundation.

A Microsoft HoloLens 2 headset and Twinbuild as a plugin for Rhino3D form the used hardware and software for augmented vaulting, respectively [67]. A construction worker supports the vault builder by managing the pair of headsets on site, uploading the digital models, and registering the markers. Augmented reality allows the mason to understand how the vault curves and to plan the brickwork details, tile cuts, and mortar joints, while foreseeing challenges ahead for a more coherent brickwork.

For overlapping the digital model on the physical site, markers are required in the form of QR codes, here printed and attached to 20 cm × 20 cm stiff boards. Relying on the precision of the production of the prefabricated timber spine, the markers are positioned on the legs at reference points, 1 m to 2 m apart, along each of the three sides of the spine, four per side. The markers are positioned as close as possible to the vault, facing the mason during construction to minimize their movement for easier registration while building. The variable brightness and lack of contrast around the vault and throughout the day can make marker registration harder, which can be improved with an integrated or external shading device.

4.4.2. Digital model

The digital model, as shown from the builder's point-of-view in Fig. 15, consists of a set of elements positioned at the intrados of the vault to form the digital guidework, in the same way that a physical guidework would have been positioned, and for easier visualization:

- the first set of curves in yellow and green represent the interface between masonry brick courses;
- the second set of curves in white, transverse to the previous ones, are not meant to show the discretization of the courses but help better visualize the double curvature of the surface;
- rectangular surfaces in grey show the specific position of the transverse tiles of the loxodromes;
- outlines of the spine help judge the alignment precision and notice drifts suggesting the need to register the model again.

While the builder mainly understands the model as a surface based on the network of curves when working on the standard parts of the tessellation of the vault, it is important to highlight the irregular parts, here the loxodrome tiles, to help the mind shift from *surface thinking*, following the general shape, to *tessellation thinking*, following the detailed brickwork, which requires more specific cognitive focus. To do so, only the loxodrome tiles are highlighted with shaded surfaces, not just outline curves.

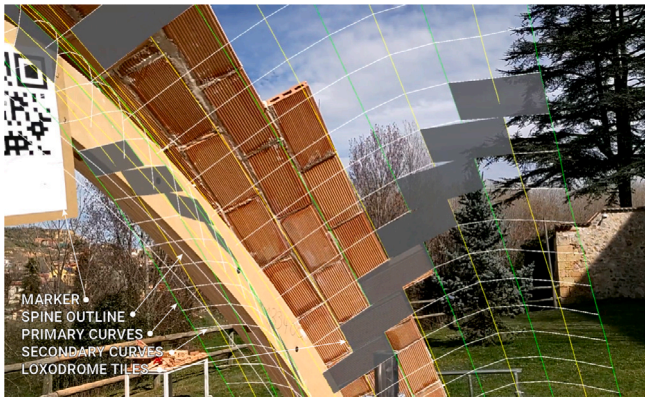

Fig. 15. Digital guidework seen from the builder's point-of-view.

4.5. Construction sequence

The gypsum plaster sets fast enough to hold a cantilevering lightweight tile, even up to 5–10 tiles that form the beginning of an arch. However, adding too many tiles, particularly the most horizontal ones, needs to be delayed to give the plaster time to set, although the loxodrome tiles add strength that does not rely on the early-age properties of the arch being built. Therefore, the arches are built in a staggered manner by starting to build the base of an arch before the previous one is closed to avoid delays. Widening the base as early as possible also provides additional stability to the structure during the assembly process. Alternation of construction between the three sides of the vault, building two to three arches on one side before shifting to another, limits the non-funicular loading of the timer spine. Therefore, the assembly sequence generally followed the main steps used for form finding, as detailed in Fig. 16. Assembling the second layer of the vault started after completing half of the first layer, progressing in parallel, to be able to reach the top of the vault from outside using a standard scaffolding for the builders. The second layer, consisting of thick bricks in a bed of cement mortar, adds weight to the first layer but contributes to the stability of the vault.

Fig. 17 summarizes construction with a timelapse of the key steps of the assembly process: assembly of the spine, construction of the base of

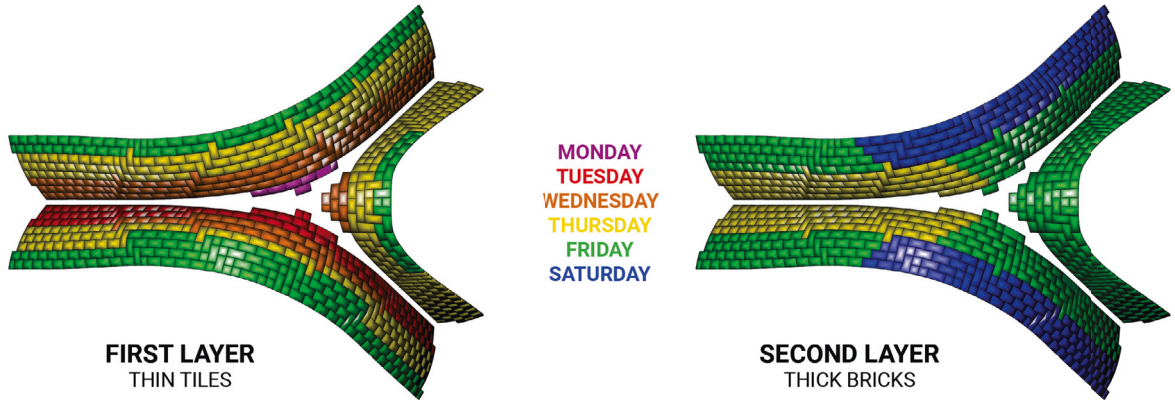

Fig. 16. Actual construction sequence of the two layers of the vault.

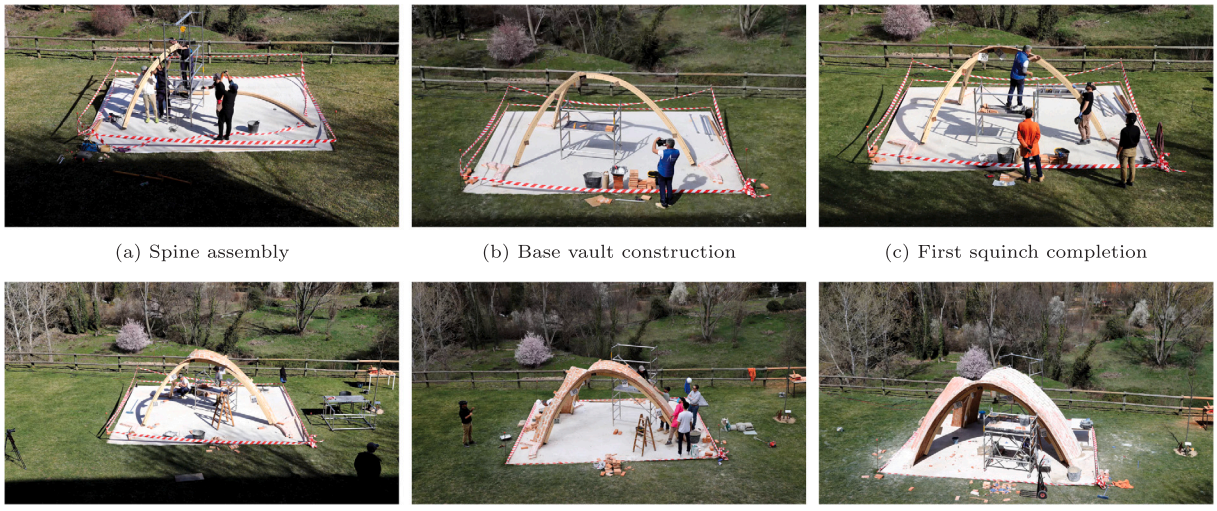

(a) Spine assembly (b) Base vault construction (c) First squinch completion

(d) First arch completion (e) Second layer construction (f) Vault cleaning

Fig. 17. Timelapse of the key steps of the construction process.

the vault, the squinches, the continuous arches, the second layer, and cleaning of the vault.

5. Falsework economy analysis

The results in terms of economy for the demonstrator are used to verify and validate the integrated design and construction approach used to minimize falsework. Firstly, the construction performance of the prototype is evaluated by considering mass, carbon, and cost of material and labor. The distribution of these factors between the different materials of the structure (the vault), and the falsework (the spine) are examined. Secondly, the falsework economy resulting from the respective implementation of each strategy (thin-tile vaulting, digital guidework, and prefabricated spine) is assessed. This impact is quantified through the mass and number of elements of falsework as proxies for measuring complexity, time, and cost. The reinforced concrete slab is excluded from the calculations because the same foundation is considered for the different alternative construction scenarios. The costs of the AR hardware (HoloLens 2 for 3849 €) and software (Fologram for 250 €/month) are excluded as to be shared across projects.

5.1. Cost calculation

The financial and environmental costs are calculated to provide the distribution between structure and falsework, material and labor. The material quantities are assessed before multiplying them by their respective unit costs. The work hours per trade are evaluated before multiplying them by their respective pay rates.

5.1.1. Material-related costs

The material-related costs are based on the volume and mass of the different materials, their unit price, and embodied carbon. The volume of materials is based on the theoretical model of the vault, using the as-designed form with a constant thickness, reported in Table 1. The prices are based on the real expenses of the project in the context of building on the campus of IE University in Segovia, Spain, in March 2023. The embodied carbon is used as a proxy for the environmental impact of the project. The embodied carbon is reported for the cradle-to-gate production stage modules A1 (raw material extraction) to A3 (manufacturing) [68,69], which usually represents up to 50% of the total carbon, and even 90% of the embodied carbon when excluding operational carbon [70], which is null in the case of this pavilion. The rest of the embodied carbon stems from the construction process (transport and installation), and end-of-life (related to demolition or deconstruction and potential beyond-life-cycle benefits), but is not accounted for. The embodied carbon values are provided by the Inventory of Carbon and Energy V3.0 [71]. The results are detailed in Table 3, providing the unit values and related assumptions.

Fig. 18 highlights the mass, cost, and carbon distribution among the materials of the structure (tiles, plaster, bricks, and mortar), and falsework (stay-in-place spine timber legs and steel connectors). Whereas

Table 3
Material-related financial cost and embodied carbon (EC).

		Mass [kg]	Unit cost [€/kg]	Cost [€]	Unit EC[a] [$kgCO_2e/kg$]	EC[a] [$kgCO_2e$]
Vault	Thin hollow clay tiles[b]	436	0.28	120	0.213	93
	Gypsum plaster[c]	140	0.15	21	0.13	18
	Thick solid clay bricks[d]	1173	0.37	434	0.213	250
	Cement mortar[e]	163	0.08	13	0.16	26
	Subtotal	**1912**	–	**588**	–	**387**
Spine	Timber plates[f]	77	5.17	398	0.681	52
	Steel plates[g]	22	16.24	350	2.46	53
	Subtotal	**99**	–	**748**	–	**105**
Total		**2011**	–	**1336**	–	**492**

[a] Cradle-to-gate embodied carbon (A1 to A3 modules) based on ICE Embodied Carbon Database V3.0 [71].
[b] Theoretical volume. Average UK EC. Waste not included.
[c] Waste not included.
[d] Theoretical volume. Average UK EC. Waste not included.
[e] Theoretical volume. EC for 1:4 CEM I cement:sand mortar. Waste not included.
[f] EC plywood without carbon capture. Waste not included. The density of plywood is taken as 0.7 t/m^3.
[g] World average EC without recycling. Waste not included. The density of steel is taken as 7.85 t/m^3.

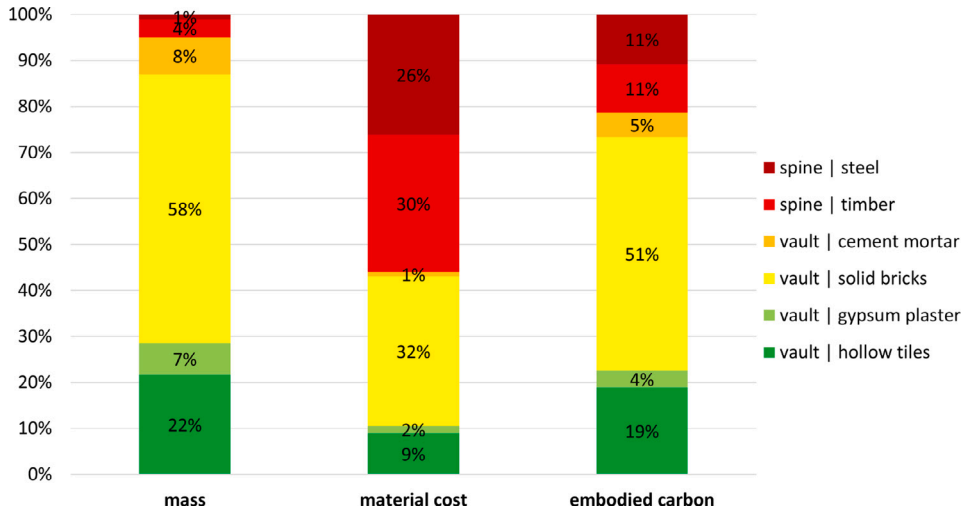

Fig. 18. Mass, material cost, and embodied carbon distribution within structural and falsework materials.

the vault represents 95% of the mass and the spine only 5%, the material cost is more even with a majority for the spine (56%), compared to the vault (44%). This is due to the low cost of the masonry materials as opposed to the CNC-produced plates, which also result in significant waste, with an even distribution between the timber arches (30%) and the steel connectors (26%). The embodied carbon mostly stems from the fired clay bricks and tiles (70%). The spine represents 22% of the embodied carbon though only 5% of the mass. Particularly, the steel connectors represent 11% of the embodied carbon for only 1% of the mass.

5.1.2. Labor-related costs

The labor-related costs are based on the construction work hours per trade, or skill, and their pay rate: expert vault builder, construction worker in charge of digital technology for augmented construction, and general construction worker. Table 4 provides the detailed hours and pay rates, resulting in labor-costs for the vault and the spine. The labor-related costs per skill, vault construction, digital construction, and general construction, are 42%, 31%, and 27%, respectively.

5.1.3. Summary

The cradle-to-gate embodied carbon footprint of the masonry vault and its timber spine is 492 $kgCO_2e$, or 54 $kgCO_2e/m^2$ of covered area. As a reference, though serving a different function, the cradle-to-gate embodied carbon footprint of concrete floors like a flat slab, a waffle slab, and a vault are 140 $kgCO_2e/m^2$, 120 $kgCO_2e/m^2$, and 75 $kgCO_2e/m^2$, respectively [72]. The spine can be mechanically optimized, its cross-section reduced, as highlighted by the measured low displacements, reducing the contribution of the falsework materials to the embodied carbon, which accounts here for 22%, and potentially be removed and repurposed instead of being a stay-in-place falsework.

The material- and labor-related costs are aggregated in Table 5 and illustrated in Fig. 19, resulting in 321 €/m^2 of covered space. The vault (structure) and the spine (falsework) represent 84% and 16% of the total cost, respectively. The labor cost represents 75%, with 73% for the vault and 2% for the spine. To make the construction of low-carbon vaults more affordable, tackling productivity and labor is essential. Adding augmented reality to the responsibility of a general construction worker and considering the standard pay rate of 20 €/h for all working hours [73], would result in a vault labor cost of 160 €/m^2, closer to the classic range of 100–120 €/m^2. A new cost distribution would then be 65%, 18%, 14%, and 2% for vault labor, material labor, vault material, and spine labor, respectively.

5.2. Economy assessment

The economy is evaluated to highlight the contributions of the different construction technologies leveraged, namely thin-tile vaulting, digital guidework, and prefabricated spine, by comparing them with alternative masonry vault falsework scenarios of scaffold, centering, and guidework.

Table 4
Labor-related financial costs.

	Vault construction			Digital construction			General construction			Total	
	Time [h]	Pay rate [€/h]	Cost [€]	Time [h]	Pay rate [€/h]	Cost [€]	Time [h]	Pay rate [€/h]	Cost [€]	Time [h]	Cost [€]
Vault[a]	42	40	1680	42	30	1260	49	20	980	133	3920
Spine[b]	0	0	0	0	0	0	5	20	100	5	100
Total	42	–	1680	42	–	1260	54	–	1080	**138**	**4020**

[a] 6 7-h days with 1 vault builder and 1 digital technology construction assistant and 1 general construction assistant + 1 extra 7-h day for general construction.
[b] 1 worker for 2 h for pre-assembly and 3 workers for 1 h for on-site installation.

Table 5
Aggregated material and labor cost for the structure and falsework per vault surface.

[€/m^2]	Vault	Spine	Total
Material	35	45	80
Labor	235	6	241
Total	270	51	**321**

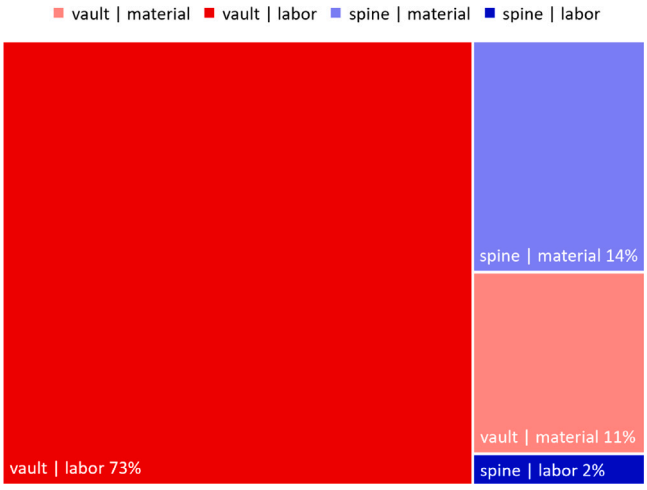

Fig. 19. Total financial cost distribution.

5.2.1. Approach

To assess the falsework economy made in construction time and cost of centering and guidework, alternative scenarios are considered to break down the contributions of the three strategies that were combined, thin-tile vaulting, digital guidework, and prefabricated spine. To avoid inferring construction time and labor, the mass and number of elements of falsework saved are used as proxy metrics to compare the different scenarios, as surrogates to transport and assembly costs. The time saved thanks to augmented reality for on-site position control is not taken into account. The time spent on digital design and construction is not taken into account either. Such information can be smoothly obtained from a digital model stemming from the design process, becoming increasingly mandatory in the context of Building Information Modeling in some countries [74].

5.2.2. Scenarios

Four construction scenarios with different falsework are illustrated in Fig. 20 with cube units that represent their falsework components.

1. **Full centering**: vault centering with scaffolding and formwork, illustrated in Fig. 20(a), as in projects like [75].
   - The standard reusable aluminum scaffolding consists of a tubular frame with cube units with a 50 cm horizontal spacing, a 100 cm vertical spacing, a 5 cm diameter, a 0.5 cm wall thickness, and bracing on each face. It results in 20 elements and 29 kg/m^3 per unit of enclosed volume.
   - The custom plywood timber waffle frame supported by the scaffolding consists of elements with a 50 cm spacing, a 20 cm depth, and a 5 cm thickness. It results in 8 elements and 14 kg/m^2 per unit of covered area.
   - The custom plywood timber planks have a 5 cm thickness, a 20 cm width, and a 200 cm length. It results in 2.5 elements and 35 kg/m^2 per unit of vault surface.
2. **Thin-tile vaulting**: boundary centering and physical vault guidework with scaffolding, illustrated in Fig. 20(b), as in projects like [9,50]. Additionally to the aluminum scaffolding and the boundary centering, boundary shoring and physical guidework are required for this scenario.
   - The boundary shoring outside the scaffolding that supports the boundary centering consists of reusable aluminum tubes with a 1 m spacing, a 5 cm diameter, a 0.5 cm wall thickness, and an inclination of 30°. It results in 1 element and 4.4 kg/m per unit of boundary arch length.
   - The guidework consists of 10 mm diameter continuous solid plastic rods that sit on the scaffolding. It results in a total of 21 elements and 0.5 kg/m^2 per unit of covered area.
3. **Thin-tile vaulting and digital guidework**: boundary centering with scaffolding, illustrated in Fig. 20(c).
   - The guidework is removed and the scaffolding is simplified to support the boundary centering only. It results in 10.7 elements and 19.8 kg/m per unit of projected boundary arch length.
4. **Thin-tile vaulting, digital guidework, and funicular spine**: prefabricated central rib centering only, illustrated in Fig. 20(d).
   - The sole centering is the stay-in-place spine, without support or shoring as the spine is form found to work mainly in compression during symmetrical assembly. It results in 2.5 elements and 3.5 kg/m per unit of spine arch length.

If the centering was to be placed on the boundary, the form would be modified to make this centering planar, like the spine, for fabrication reasons. Indeed, single or double curvature timber requires access to more complex fabrication technology with an increase in cost ratio of 5 to 15 compared to planar elements, respectively [76]. Therefore, a planar boundary centering is considered, with the same length as the actual doubly-curved boundary and the average height of the vault. Additional mobile scaffolding or device like a cherry picker for access and reachability for construction workers is not considered, as necessary for all these scenarios. Comparing scenarios 1 and 2 provides the falsework economy made with thin-tile vaulting, scenarios 2 and 3 the one with digital guidework, and scenarios 3 and 4 the one with funicular spine.

5.2.3. Results

Table 6 summarizes the quantity of falsework for each alternative construction scenario, while Table 7 provides the detailed values per falsework element. The mass and number of elements of falsework

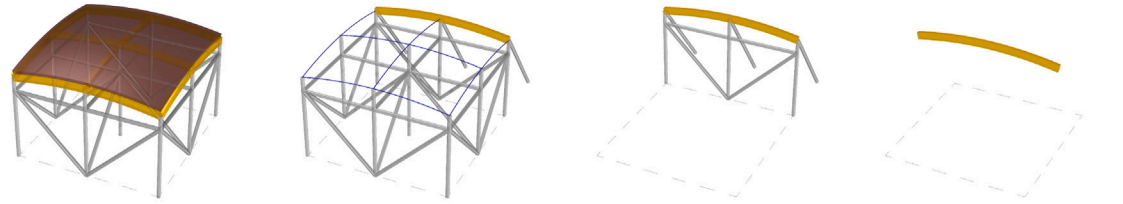

(a) Vault centering with scaffolding and formwork (b) Boundary centering and physical guidework (c) Boundary centering and digital guidework (d) Prefabricated central rib centering

Fig. 20. Illustration of alternative falsework scenarios.

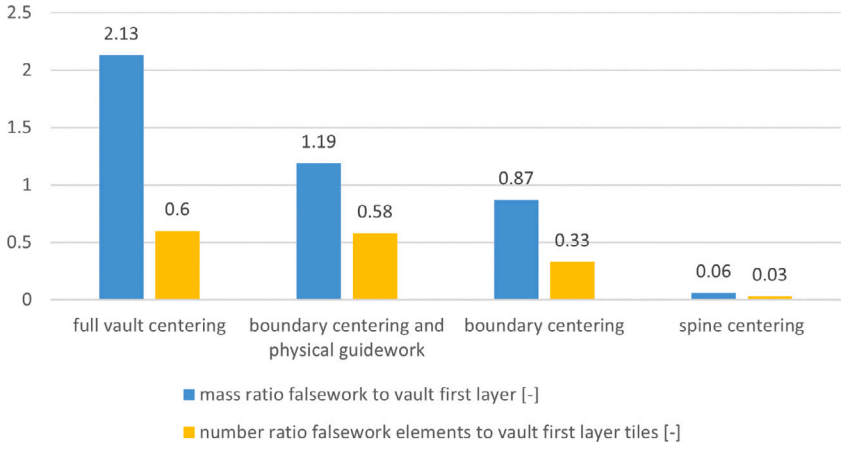

Fig. 21. Falsework to structure quantity ratios per alternative construction scenario.

Table 6
Falsework quantities per alternative construction scenario.

Scenario	Mass [t]	Elements [–]
1 - Full vault centering	1.19	443
2 - Boundary centering and physical guidework	0.66	431
3 - Boundary centering and digital guidework	0.48	244
4 - Spine centering and digital guidework	0.04	26

are normalized by 558 kg, the mass of the first layer of the vault, and 742, the theoretical number of tiles in the first layer of the vault, respectively. Fig. 21 shows that in scenario 1, without efforts to reduce falsework, the falsework mass is more than double the one of the first layer of the actual vault, scenarios 2 and 3 reduce it to ratios around 1, and scenario 4, which is the actually implemented one, has a ratio as low as 6%. Similarly, scenario 1 necessitates a ratio of elements of 60%, as opposed to 3% for scenario 4.

Table 8 extracts the falsework economy made due to each construction strategy leveraged for this prototype: thin-tile vaulting, digital guidework, and funicular spine. Fig. 22 shows their relative contribution in falsework reduction. Regarding the economy of falsework mass, thin-tile vaulting has the most impact by removing the custom timber centering (46%). Then, prefabricated spine has the second most impact by removing the scaffold (39%). Regarding the economy of falsework elements, digital guidework (45%) and prefabricated spine (52%) enable the removal of most of the falsework elements. Their relative contributions depend on the area-to-perimeter ratio of the vault. Scaling up the size of the vault increases this ratio and therefore the contribution of digital guidework.

5.3. Benchmark

These results are benchmarked against the construction of other thin-tile vaults in the literature.

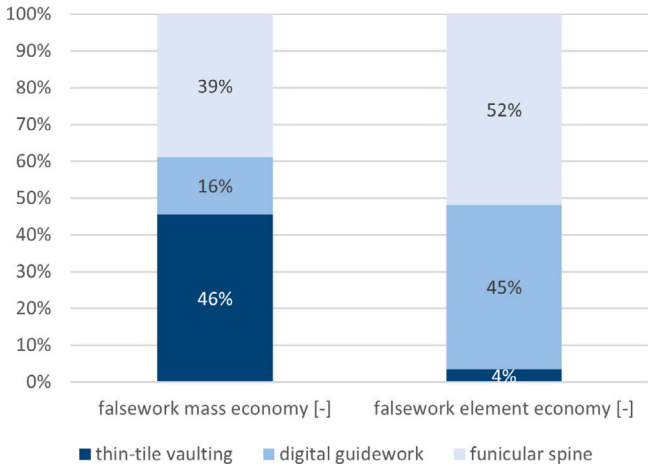

Fig. 22. Falsework economy per construction strategy.

Davis et al. [8] built a thin-tile vault with a centering made of reusable standard wood palettes and single-use custom cardboard boxes produced using a CNC. For this 3.5 t vault, the falsework weighted 2.8 t, or 85% of the mass of the vault itself. An estimated 1.2 t for the first layer of the vault (28.6 m^2 of vault surface with 1 kg tiles of 200 mm × 120 mm × 40 mm) yields a mass ratio falsework to vault first layer of 2.3, higher than any of the alternative scenarios considered in Fig. 21. Bricklaying took 42.5 work-hours for a vault surface of 28.6 m^2, or 1.5 h/m^2, to compare with 2.0 h/m^2 to produce the 16.7 m^2 in 33 work-hours for the innixAR demonstrator.

For a large-scale vault, Ramage et al. [77] used a centering of flat timber arches on the boundary and then a lightweight radial guidework for the central part. The vaults cost 200 $/$m^2$ of material and labor, in Rwanda in 2017, with a finished interior but excluding waterproofing

Table 7
Falsework element unit metrics.

Falsework	Dimension	Unit x	Value	Volume density [dm^3/x]	Mass density [kg/x]	Element density [-/x]	Total volume [dm^3]	Total mass [kg]	Total elements [–]
Scaffold[a]	Enclosed volume	[m^3]	16.4	10.7	29.0	20.0	176	475	328
Beams[b]	Covered area	[m^2]	9.2	20.0	14.0	8.0	184	129	74
Planks[c]	Vault surface	[m^2]	16.7	50.0	35.0	2.5	835	585	42
Splines[d]	Covered area	[m^2]	9.2	0.3	0.5	2.3	3	4	21
Boundary scaffold[e]	Projected boundary arch length	[m]	15.2	7.3	19.8	10.7	111	301	163
Boundary centering[f]	Boundary arch length	[m]	23.3	5.0	3.5	2.5	117	82	58
Boundary shoring[g]	Boundary arch length	[m]	23.3	1.6	4.4	1.0	38	102	23
Spine[f]	Spine length	[m]	10.2	5.0	3.5	2.5	51	36	26

The densities of aluminum, plywood, and plastic are taken as 2.7 t/m^3, 0.7 t/m^3, and 1.5 t/m^3, respectively.

[a] Reusable aluminum frame with cube units with a 50 cm horizontal spacing, a 100 cm vertical spacing, a 5 cm diameter tubes with a 0.5 cm wall thickness and bracing on each face.

[b] Custom plywood timber waffle frame with a 50 cm spacing, a 20 cm depth, and a 5 cm thickness.

[c] Custom plywood timber planks with a 5 cm thickness, a 20 cm width, and a 200 cm length.

[d] Plastic continuous solid rods with a 10 mm diameter.

[e] Single-direction aluminum scaffold.

[f] Custom 5-layer plywood plate elements with 2 m average length.

[g] Reusable aluminum tubes with a 1 m spacing, a 5 cm diameter, a 0.5 cm wall thickness, and an inclination of 30°.

Table 8
Falsework economy per construction strategy.

Construction strategy	Falsework mass [t]	Falsework nb. elements [–]
Thin-tile vaulting	0.53	13
Digital guidework	0.18	187
Prefabricated spine	0.45	219

and covering. A cost comparable to a previous project in South Africa in 2010 that cost 130 $/m^2, or 190 $/m^2 when taking into account inflation [78]. Taking into account inflation, 200 $/m^2 in January 2017 corresponds to 250 $/m^2 or 225 €/m^2 in January 2023, to be compared with the cost of the innixAR demonstrator of 270 €/m^2, or 321 €/m^2 including falsework, made in Spain in Winter 2023. Making this approach and technology more widespread in the construction industry would allow considering the standard flat pay rate of 20 €/h [73], meaning a cost of 160 €/m^2 for the construction of the vault.

This assessed falsework economy, enabled by 4D funicular design with craft and digital construction technologies, shows a promising reduction in falsework material, labor, and cost, which still needs to be scaled in terms of project size and labor skill to show a large impact in the construction industry.

6. Conclusion

This paper presented an integrated design and construction approach to minimize falsework in the construction of masonry vaults, which are usually mechanically efficient but expensive structures to build. Several historical and digital construction technologies were leveraged, namely thin-tile vaulting, loxodrome tessellation, digital guidework, and prefabricated spine. This construction process informed 4D funicular design to obtain the form, tessellation, thickness, and assembly sequence. This approach was validated with the construction of the innixAR demonstrator, where the only falsework is a stay-in-place prefabricated timber spine. An analysis of the falsework economy found that falsework represented only 4% of the construction time, 2% of the labor cost, and 14% of the material cost. Thin-tile vaulting and prefabricated spine allowed a reduction in 82% of the falsework mass to transport, whereas digital guidework and prefabricated spine allowed a reduction in 91% of the falsework elements to assemble, compared to a full vault centering as a benchmark. This paper contributed to the development of structures that are efficient both mechanically and constructionally. Testing this approach on larger projects and training masonry vault builders will be essential to scale within the construction industry the impact of such falsework economy.

CRediT authorship contribution statement

Robin Oval: Conceptualization, Data curation, Formal analysis, Investigation, Methodology, Software, Validation, Writing – original draft, Visualization. **Rafael Pastrana:** Conceptualization, Data curation, Formal analysis, Investigation, Methodology, Software, Validation, Visualization, Writing – original draft. **Edvard P.G. Bruun:** Conceptualization, Investigation, Methodology, Writing – review & editing. **Vittorio Paris:** Conceptualization, Investigation, Methodology, Validation, Writing – review & editing. **Salvador Gomis Aviño:** Investigation, Methodology, Validation. **Sigrid Adriaenssens:** Conceptualization, Funding acquisition, Project administration, Resources, Supervision, Writing – review & editing. **Wesam Al Asali:** Conceptualization, Funding acquisition, Investigation, Methodology, Project administration, Resources, Supervision, Validation, Visualization, Writing – original draft.

Declaration of competing interest

The authors declare that they have no known competing financial interests or personal relationships that could have appeared to influence the work reported in this paper.

Acknowledgments

The authors would like to thank Carlo Olivieri and Orsolya Gáspár for their feedback on the project, as well as the technical, media, and administrative teams of IE University for their support. The authors would also like to thank La Paloma Cerámicas for their generous donation of the tiles and bricks, and Twinbuild for their precious technical support. This research was partially funded by the U.S. National Science Foundation grants 2122271 and OAC-2118201, and Princeton University's Institute for International and Regional Studies (PIIRS), United States.

References

[1] Barbosa Filipe, Woetzel Jonathan, Mischke Jan, Ribeirinho Maria Jao, Sridhar Mukund, Parsons Matthew, Bertram Nick, Brown Stephanie. Reinventing construction through a productivity revolution. Technical report, McKinsey Global Institute; 2017.

[2] Organization International Labour. The construction industry in the twentyfirst century: Its image, employment prospects and skill requirements. Technical report, Geneva: International Labour Organization; 2001.

[3] Hanna Awad S. Concrete formwork systems. 1st ed.. Boca Raton: CRC Press; 1998, URL https://doi.org/10.1201/9780203909690.

[4] Lab Robert H. Think formwork - Reduce costs. Struct Mag 2007;14–6, URL https://www.structuremag.org/?p=6139.

[5] Heyman Jacques. The Stone Skeleton: Structural engineering of masonry architecture. 1st paperback ed.. New York, NY: Cambridge Univ. Press; 1997, ISBN: 978-0-521-62963-8 978-0-521-47270-8.

[6] Heyman Jacques. Equilibrium of shell structures. Oxford engineering science series, Oxford [Eng.]: Clarendon Press; 1977.

[7] Fitchen John. The construction of Gothic cathedrals: A study of medieval vault erection. Chicago: University of Chicago Press; 1981.

[8] Davis Lara, Rippmann Matthias, Pawlofsky Tom. Innovative funicular tile vaulting: A prototype vault in Switzerland. Struct Eng 2012.

[9] López López David, Domènech Rodríguez Marta, Palumbo Fernández Mariana. "Brick-topia", the thin-tile vaulted pavilion. Case Stud Struct Eng 2014;2:33–40. http://dx.doi.org/10.1016/j.csse.2014.09.001.

[10] Woolley Leonard. Ur of the Chaldees: A record of 7 years of excavation. 1st ed.. London: Ernest Benn; 1929.

[11] Benvenuto Edoardo, Corradi Massimo. La statica delle false volte. In: Architettura in pietra a secco. Atti del 1°seminario internazionale. Schena Editore; 1987, p. 93–106.

[12] Fraddosio Aguinaldo, Lepore Nicola, Piccioni Mario Daniele. Further refinement of the corbelling theory for the equilibrium analysis of corbelled domes. Curv Layer Struct 2019;6(1):30–40. http://dx.doi.org/10.1515/cls-2019-0003.

[13] von Pilgrim Cornelius, Mueller Wolfgang, el-Bialy Mohamed. Report on the eleventh season of the joint Swiss-Egyptian Mission in Syene/Old Aswan (2010/2011). Technical report, Swiss Institute of Architectural and Archaeological Research on Ancient Egypt, Cairo; 2011, URL http://swissinst.ch/downloads/Report%20on%20the%20Eleventh%20Season%20of%20the%20Joint%20Swiss_Egyptian%20Mission%20in%20Syene_Old%20Aswan%20(2010_2011).pdf.

[14] Choisy Auguste. L'Art de bâtir chez les Byzantins. Paris: Société Anonyme De Publications Périodiques; 1883.

[15] Huerta Santiago. The geometry and construction of Byzantine vaults: the fundamental contribution of Auguste Choisy. In: Auguste Choisy (1841-1909): l'architecture et l'art de bâtir. Universidad Politécnica de Madrid; 2009, p. 289–305.

[16] Lancaster Lynne C. Complex vault forms of brick. In: Innovative vaulting in the architecture of the Roman empire: 1st to 4th centuries CE. Cambridge: Cambridge University Press; 2015, p. 70–98. http://dx.doi.org/10.1017/CBO9781107444935.005.

[17] Fathy Hasan. Architecture for the poor: An experiment in rural Egypt. Nachdr. ed.. Chicago, Ill.: Univ. Press; 1973.

[18] Guastavino Rafael. Essay on the theory and history of cohesive construction: Applied especially to the timbrel vault. Ticknor and Company, Boston; 1893.

[19] López López David, Van Mele Tom, Block Philipe. La bóveda tabicada en el siglo XXI. Inf Constr 2016;68(544):162. http://dx.doi.org/10.3989/ic.15.169.m15.

[20] Al Asali Mohammad Wesam. Craft-inclusive construction: Design strategies for thin-tile vaulting (PhD thesis), University of Cambridge; 2020, URL https://www.repository.cam.ac.uk/handle/1810/322971.

[21] Arce Ignacio. From the diaphragm arches to the ribbed vaults. An hypothesis for the birth and development of a building technique. In: Proceedings of the first international congress on construction history. Madrid; 2003, p. 225–41, URL http://www.sedhc.es/biblioteca/actas/CIHC1_023_Arce%20I.pdf.

[22] Fuentes Paula, Huerta Santigao. Islamic domes of crossed-arches: Origin, geometry and structural behavior. In: 6th international conference on arch bridges. Fuzhou, China; 2010, p. 346–53, URL https://oa.upm.es/4626/.

[23] Alkadi Rana M. The origin of the Islamic ribbed vaults famed in North Africa and Spain (PhD thesis), Universidad Politécnica de Madrid; 2017, URL http://oa.upm.es/47687/.

[24] Askarov Shukur. Amir Temur and Philippe Brunelleschi. 2004, URL https://sanat.orexca.com/2004/2004-3/history_art5/.

[25] Mainstone Rowland J. Brunelleschi's dome of Santa Maria del Fiore and some related structures. Trans Newcom Soc 1969;42(1):107–26. http://dx.doi.org/10.1179/tns.1969.006.

[26] Paris Vittorio, Pizzigoni Attilio, Adriaenssens Sigrid. Statics of self-balancing masonry domes constructed with a cross-herringbone spiraling pattern. Eng Struct 2020;215:110440. http://dx.doi.org/10.1016/j.engstruct.2020.110440.

[27] Fisher Clarence S. The minor cemetery at Giza. Philadelphia: University Museum; 1924, URL http://www.gizapyramids.org/pdf_library/fisher_minor_cemetery.pdf.

[28] Lancaster Lynne C. Vaulting tubes. In: Innovative vaulting in the architecture of the Roman empire: 1st to 4th centuries CE. Cambridge: Cambridge University Press; 2015, p. 99–128, URL https://doi.org/10.1017/CBO9781107444935.006.

[29] Gallon Jean-Gaffin. Machines et inventions approuvées par l'Academie royale des Sciences. vol. 2, Paris: Martin-Coignard-Guerin; 1735, URL ark:/12148/bpt6k3476b.

[30] Lassaulx Johann Klaudius von. Beschreibung des Verfahrens bei Anfertigung leichter Gewölbe über Kirchen und ähnliche Räumen. In: Journal für die Baukunst. Berlin: G. Reimer; 1829, p. 317–30, URL https://doi.org/10.11588/diglit.19234.35.

[31] Bruun Edvard PG, Oval Robin, Al Asali Wesam, Gaspar Orsolya, Paris Vittorio, Adriaenssens Sigrid. Automating historical centering-minimizing masonry vaulting strategies: Applications to cooperative robotic construction. Autom Constr 2024. in press.

[32] Dörfler Kathrin, Sandy Timothy, Giftthaler Markus, Gramazio Fabio, Kohler Matthias, Buchli Jonas. Mobile robotic brickwork. In: Reinhardt Dagmar, Saunders Rob, Burry Jane, editors. Robotic fabrication in architecture, art and design 2016. Cham: Springer International Publishing; 2016, p. 204–17. http://dx.doi.org/10.1007/978-3-319-26378-6_15, URL http://link.springer.com/10.1007/978-3-319-26378-6_15. ISBN: 978-3-319-26376-2 978-3-319-26378-6.

[33] Goessens Sébastien, Mueller Caitlin, Latteur Pierre. Feasibility study for drone-based masonry construction of real-scale structures. Autom Constr 2018;94:458–80. http://dx.doi.org/10.1016/j.autcon.2018.06.015, URL https://linkinghub.elsevier.com/retrieve/pii/S0926580518301961.

[34] Parascho Stefana, Han Isla Xi, Walker Samantha, Beghini Alessandro, Bruun Edvard PG, Adriaenssens Sigrid. Robotic vault: A cooperative robotic assembly method for brick vault construction. Constr Robot 2020;4(3):117–26. http://dx.doi.org/10.1007/s41693-020-00041-w.

[35] Han Isla Xi, Bruun Edvard PG, Marsh Stuart, Adriaenssens Sigrid, Parascho Stefana. From concept to construction: A transferable design and robotic fabrication method for a building-scale vault. In: Proceedings of the 40th annual conference of the association for computer aided design in architecture. Online; 2020, p. 614–23, URL http://papers.cumincad.org/cgi-bin/works/Show?acadia20_614.

[36] Parascho Stefana, Han Isla Xi, Beghini Alessandro, Miki Masaaki, Walker Samantha, Bruun Edvard PG, Adriaenssens Sigrid. LightVault: A design and robotic fabrication method for complex masonry structures. In: Advances in architectural geometry 2020. Paris, France: Presses des Ponts; 2021, p. 350–75, URL https://thinkshell.fr/wp-content/uploads/2019/10/AAG2020_18_Parascho.pdf.

[37] Bruun Edvard PG, Pastrana Rafael, Paris Vittorio, Beghini Alessandro, Pizzigoni Attilio, Parascho Stefana, Adriaenssens Sigrid. Three cooperative robotic fabrication methods for the scaffold-free construction of a masonry arch. Autom Constr 2021;129:103803. http://dx.doi.org/10.1016/j.autcon.2021.103803.

[38] Mitterberger Daniela, Dörfler Kathrin, Sandy Timothy, Salveridou Foteini, Hutter Marco, Gramazio Fabio, Kohler Matthias. Augmented bricklaying: Human–machine interaction for in situ assembly of complex brickwork using object-aware augmented reality. Constr Robot 2020;4(3–4):151–61. http://dx.doi.org/10.1007/s41693-020-00035-8, URL https://link.springer.com/10.1007/s41693-020-00035-8. ISSN: (2509-811X, 2509-8780).

[39] Fazel Alireza, Izadi Abbasali. An interactive augmented reality tool for constructing free-form modular surfaces. Autom Constr 2018;85:135–45. http://dx.doi.org/10.1016/j.autcon.2017.10.015, URL https://linkinghub.elsevier.com/retrieve/pii/S0926580516302497.

[40] Fazel Alireza, Fayaz Rima, Mostaghni Alireza, Matini Mohammad Reza. Optical tool for additive construction of complex brick structures. Autom Constr 2022;140:104330. http://dx.doi.org/10.1016/j.autcon.2022.104330, URL https://linkinghub.elsevier.com/retrieve/pii/S0926580522002035.

[41] Song Yang, Koeck Richard, Agkathidis Asterios. Augmented Bricklayer: An augmented human-robot collaboration method for the robotic assembly of masonry structures. In: SiGraDi. 2022.

[42] Oliva Salinas Juan Gerardo. UNAM Vault. 2022, URL https://docs.fologram.com/d3fb2cda6f6f49d994395bc08d974865#UNAM_Vault.

[43] Sàrl Pittet Artisans. Escalier sur voûte sarrasine et réalité augmentée. 2023, URL https://www.linkedin.com/posts/pittetartisans_rhino3d-grasshopper3d-fologram-activity-7064819361626116096-AVlB?utm_source=share&utm_medium=member_desktop.

[44] Collins George R. The transfer of thin masonry vaulting from Spain to America. J Soc Archit Hist 1968;27(3):176–201. http://dx.doi.org/10.2307/988501.

[45] Roberti Giulio Mirabella, Ruscica Giuseppe, Paris Vittorio. From the herringbone dome by Sangallo to the Serlio floor of Emy (and beyond). Curv Layer Struct 2021;8(1):259–70. http://dx.doi.org/10.1515/cls-2021-0023, URL https://www.degruyter.com/document/doi/10.1515/cls-2021-0023/html.

[46] Camacho Marín René. El nuevo mercado de Cunduacán. 2023, URL https://www.xevt.com/tabasco/entregara-sedatu-al-fin-nuevo-mercado-de-cunduacan/248373.

[47] Ramírez Ponce Alfonso. Arquitectura propia: Cubiertas de ladrillo recargado. 2012, URL http://ramirezponcearquitecto.blogspot.com/2012/06/arquitectura-propia-cubiertas-de.html.

[48] Ramírez Ponce Alfonso, Ramírez Melendez Rafael. Curves of clay: Mexican brick vaults and domes. In: Williams Kim, Ostwald Michael J, editors. Architecture and mathematics from antiquity to the future. Cham: Springer International Publishing; 2015, p. 309–24, URL https://doi.org/10.1007/978-3-319-00137-1_21.

[49] Guzmán Urbina Xavier, Hernández Hernández Agustín, San Martín Córdova Ivan, editors. Fernando López carmona: Arquitecto, 50 años de enseñanza. Colección arquitectura, 1st ed.. México: Universidad Nacional Autónoma de México; 2010.

[50] Borne Emmanuelle, Heathcote Edwin. The droneport project. L'Arch d'Aujourd'hui Perspect 2016.

[51] Fuentes Paula, Huerta Santiago. Crossed-arch vaults in late Gothic and early Renaissance vaulting: A problem of building technology transfer. In: Proceedings of the fifth international congress on construction history. Chicago; 2015, p. 8, URL https://oa.upm.es/36242/.
[52] Reuther Oskar. Ocheïdir: Nach aufnahmen von Mitgliedern der Babylon-expedition der deutschen Orient-Gesellschaft. Leipzig: J.C. Hinrichs; 1912, URL https://catalog.hathitrust.org/Record/002639832.
[53] Oval Robin, Rippmann Matthias, Mesnil Romain, Van Mele Tom, Baverel Olivier, Block Philippe. Feature-based topology finding of patterns for shell structures. Autom Constr 2019;103:185–201. http://dx.doi.org/10.1016/j.autcon.2019.02.008, URL https://linkinghub.elsevier.com/retrieve/pii/S0926580518304321.
[54] Blum Harry. A transformation for extracting new descriptors of shape. In: Models for the perception of speech and visual form. MIT Press; 1967, p. 362–80.
[55] Kao Gene T C, Körner Axel, Sonntag Daniel, Nguyen Long, Menges Achim. Assembly-aware design of masonry shell structures: A computational approach. In: Proceedings of IASS annual symposium 2017. 2017.
[56] Deuss Mario, Panozzo Daniele, Whiting Emily, Liu Yang, Block Philippe, Sorkine-Hornung Olga, Pauly Mark. Assembling self-supporting structures. ACM Trans Graph 2014;33(6):1–10. http://dx.doi.org/10.1145/2661229.2661266.
[57] Block Philippe, Ochsendorf John. Thrust Network Analysis: A new methodology for three-dimensional equilibrium. J Int Assoc Shell Spatial Struct 2007;48(3).
[58] Schek Hans-Jörg. The force density method for form finding and computation of general networks. Comput Methods Appl Mech Engrg 1974;3(1):115–34. http://dx.doi.org/10.1016/0045-7825(74)90045-0, URL https://linkinghub.elsevier.com/retrieve/pii/0045782574900450.
[59] Pastrana Rafael, Oktay Deniz, Adams Ryan P, Adriaenssens Sigrid. JAX FDM: A differentiable solver for inverse form-finding. In: ICML 2023 workshop on differentiable almost everything: differentiable relaxations, algorithms, operators, and simulators. 2023, URL https://openreview.net/forum?id=Uu9OPgh24d.
[60] Pastrana Rafael, Oktay Deniz, Adams Ryan P, Adriaenssens Sigrid. JAX FDM: Auto-differentiable and hardware-accelerated force density method. 2023, http://dx.doi.org/10.5281/zenodo.7258292, URL https://github.com/arpastrana/jax_fdm.
[61] Nocedal Jorge. Updating quasi-Newton matrices with limited storage. Math Comp 1980;35(151). http://dx.doi.org/10.1090/S0025-5718-1980-0572855-7, 773–773. URL http://www.ams.org/jourcgi/jour-getitem?pii=S0025-5718-1980-0572855-7.
[62] Corliss George, Faure Christele, Griewank Andreas, Hascoet Laurent, Naumann Uwe. Automatic differentiation of algorithms: From simulation to optimization. New York, NY: Springer; 2013, URL https://link.springer.com/book/10.1007/978-1-4613-0075-5.
[63] Van Mele Tom, Panozzo Daniele, Sorkine-Hornung Olga, Block Philippe. Best-fit Thrust Network Analysis. In: Shell structures for architecture-form finding and optimization. 2014, p. 157–70.
[64] Maia Avelino Ricardo, Iannuzzo Antonino, Van Mele Tom, Block Philippe. Assessing the safety of vaulted masonry structures using Thrust Network Analysis. Comput Struct 2021;257:106647. http://dx.doi.org/10.1016/j.compstruc.2021.106647, URL https://linkinghub.elsevier.com/retrieve/pii/S0045794921001693.
[65] Marmo Francesco, Masi Daniele, Mase Daniele, Rosati Luciano. Thrust Network Analysis of masonry vaults. Int J Mason Res Innov 2019;4(1/2):64. http://dx.doi.org/10.1504/IJMRI.2019.096828, URL http://www.inderscience.com/link.php?id=96828. ISSN: (2056-9459, 2056-9467).
[66] Adiels Emil, Ander Mats, Williams Chris J K. Brick patterns on shells using geodesic coordinates. In: Proceedings of IASS annual symposium 2017. 2017.
[67] Twinbuild. Augmented reality for the construction site. 2021, URL https://twinbuild.com/.
[68] BS Standards. BS EN 15978:2011 - Sustainability of construction works. Assessment of environmental performance of buildings. Calculation method. London, UK: British Standards Institution London; 2012.
[69] BS Standards. BS EN 15804:2012+A2:2019 - Sustainability of construction works. Environmental product declarations. Core rules for the product category of construction products. London, UK: British Standards Institution London; 2021.
[70] Gibbons Orlando P, Orr John J, Archer-Jones Cameron, Arnold Will, Green Daniel. How to calculate embodied carbon. IStructE Ltd; 2022, OCLC: 1204592933.
[71] ICE. Embodied carbon - The ICE Database. 2023, URL https://circularecology.com/embodied-carbon-footprint-database.html.
[72] Oval Robin, Nuh Mishael, Costa Eduardo, Madyan Omar Abo, Orr John, Shepherd Paul. A prototype low-carbon segmented concrete shell building floor system. Structures 2023;49:124–38. http://dx.doi.org/10.1016/j.istruc.2023.01.063, URL https://linkinghub.elsevier.com/retrieve/pii/S2352012423000644.
[73] Ingenieros CYPE. Generador de precios - Estructuras - Fábrica - Bóveda de escalera. 2024, URL http://www.generadordeprecios.info/rehabilitacion/Estructuras/Fabrica/Bovedas/Boveda_de_escalera_dos_tableros.html#gsc.tab=0.
[74] French Ministry of Ecological Transition. The digital transition plan for buildings. Technical report, Ministry of Ecological Transition; 2018.
[75] Rippmann Matthias. Funicular shell design: Geometric approaches to form finding and fabrication of discrete funicular structures (PhD thesis), ETH Zurich; 2016, http://dx.doi.org/10.3929/ETHZ-A-010656780.
[76] Svilans Tom. GluLamb: A toolkit for early-stage modelling of free-form glue-laminated timber structures. In: European conference on computing in construction. 2021, p. 373–80. http://dx.doi.org/10.35490/EC3.2021.194, URL https://ec-3.org/publications/conference/paper/?id=EC32021_194.
[77] Ramage Michael, Hall Timothy J, Gatóo Ana, Al Asali M Wesam. Rwanda Cricket Stadium: Seismically stabilised tile vaults. Structures 2019;18:2–9. http://dx.doi.org/10.1016/j.istruc.2019.02.004.
[78] Ramage Michael H, Ochsendorf John, Rich Peter, Bellamy James K, Block Philippe. Design and construction of the Mapungubwe National Park interpretive centre, south africa. ATDF J 2010;7(1/2):14–23.